SSC-143

The Superconducting Super Collider

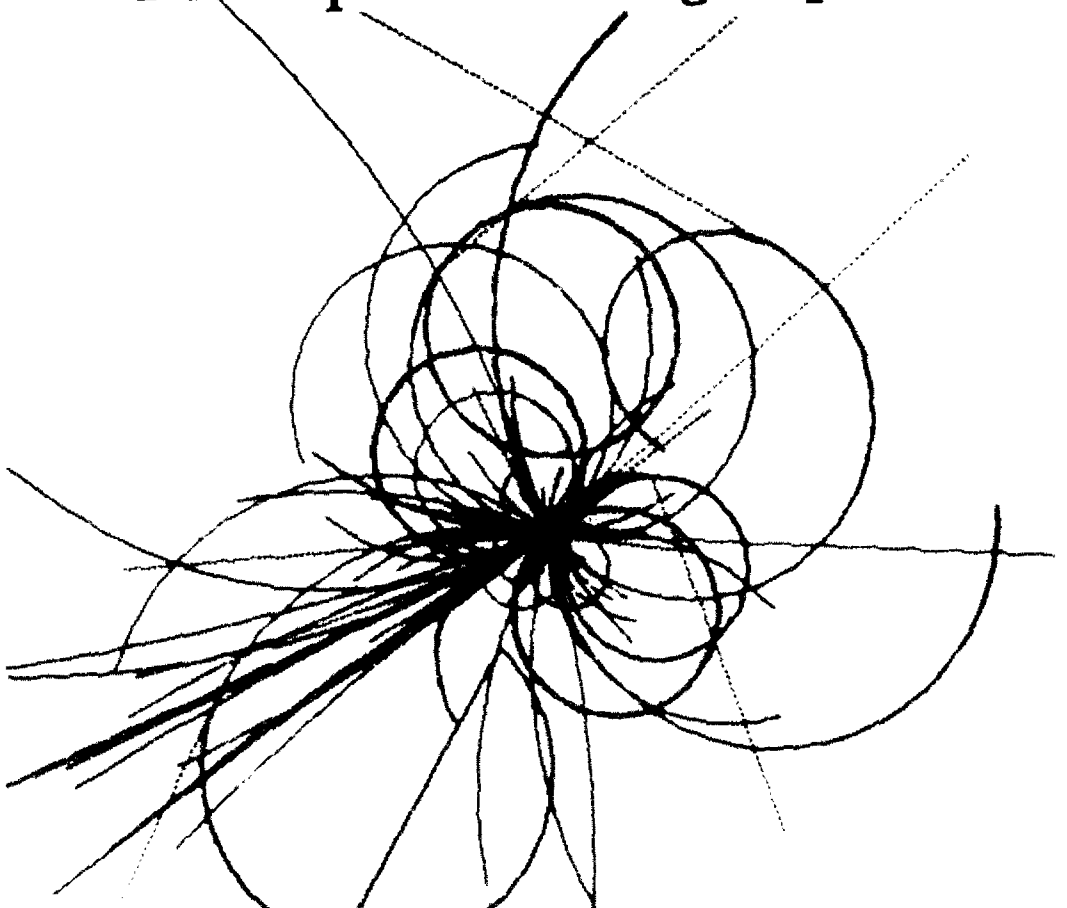

Hadron Production in Hadron-Nucleus and Nucleus-Nucleus Collisions in the Dual Monte Carlo Multi-Chain Fragmentation Model

J. Ranft
SSC Central Design Group

September 1987

SSC-143

Hadron Production in Hadron-Nucleus and Nucleus-Nucleus Collisions in the Dual Monte Carlo Multi-Chain Fragmentation Model

J. Ranft*
SSC Central Design Group†
Lawrence Berkeley Laboratory 90-4040
Berkeley, California 94720

September 1987

* Permanent address: Sektion Physik, Karl-Marx-Universität, Leipzig, G.D.R.

† Operated by the Universities Research Association for the Department of Energy.

SSC–143

28 SEPTEMBER 1987

HADRON PRODUCTION IN HADRON-NUCLEUS AND NUCLEUS-NUCLEUS COLLISIONS IN THE DUAL MONTE CARLO MULTI-CHAIN FRAGMENTATION MODEL

J. RANFT*

SSC Central Design Group, Lawrence Berkeley Laboratory,

University of California Berkeley, CA 94720

Hadron production in hadron-nucleus and nucleus-nucleus collisions is studied by a Monte-Carlo version of the dual multi-chain fragmentation model. The model takes into account leading order corrections due to the secondary interactions of low energy secondaries inside the target nucleus. An empirical formation time parameter is introduced and used to decide which secondaries interact again inside the target. Data for the multiparticle production in proton-nucleus and oxygen-nucleus interactions at 200 GeV/nucleon from different experiments are well described by the model and consistent with a formation time parameter of $\tau c = 2 \pm 1$ fm.

* Permanent address: Sektion Physik, Karl-Marx-Universität, Leipzig, G.D.R.

1. INTRODUCTION

In this paper high energy nucleon-nucleus and nucleus-nucleus collisions will be studied within one and the same model.

High energy collisions of heavy ions offer the possibility to discover experimentally the quark gluon plasma,[1] a new state of matter. Experimental studies using nuclei accelerated up to energies of 200 GeV per nucleon started in 1986 at the CERN Super Proton Synchrotron. First experimental results have become available.[2,3]

Experiments on inelastic hadron-nucleus collisions have been performed since many years. There exists numerous models which try to describe and understand the data, see Ref. 4, where the experimental and phenomenological situation is reviewed.

In order to understand, which signatures of heavy ion collisions point to the formation of a quark gluon plasma, we should study such collisions within conventional models of hadron physics for soft particle production. Scattering events predicted by such conventional models are the background against which the effects of the quark-gluon plasma have to be found.

The Monte-Carlo version of the dual multistring fragmentation model has been applied successfully to hadron-hadron collisions,[5,6] hadron-nucleus collisions[7,8] and nucleus-nucleus collisions.[9,10] The same models have also been studied using different techniques.[11–14]

In Section 2 the dual multistring fragmentation model for hadron-nucleus and nucleus-nucleus collisions will be defined. In Section 3 leading order corrections

to this model are introduced. These corrections concern secondary interactions of some of the low energy hadrons created in the collisions inside the nucleus. The concept of a formation time[15] is used in order to decide under which conditions such secondary interactions are possible. In Section 4 details about the Monte-Carlo model are given and in Section 5 the model is compared to experimental data and discussed.

2. THE DUAL MONTE-CARLO MULTI-CHAIN FRAGMENTATION MODEL

The dual Monte-Carlo multi-chain fragmentation model has been applied before to hadron-nucleus collisions[7,8] and to nucleus-nucleus collisions.[9,10] These models correspond closely to models studied by other groups[11,13,14] mainly with non-Monte-Carlo methods.

Here we implement the model both for nucleon-nucleus and nucleus-nucleus collisions.

In nucleon-nucleus and nucleus-nucleus collisions many elementary interactions can occur. In Fig. 1 we give an example for a nucleon-nucleus collision. The collisions is characterized by a total of n elementary collisions. In each elementary collision particles are produced via two multiparticle chains, therefore the total number of chains is $2n$. In each inelastic nucleon-nucleus collision the projectile nucleus ($n_p = 1$) and $n_t = n$ target nucleons take part. The multiparticle chains have either valence quarks and diquarks at their ends or sea-quark-antiquark pairs. $n-1$ sea quark pairs of the projectile nucleon are needed

to form the chains. The elementary collisions can be classified as valence-valence and valence-sea collisions.

In nucleus-nucleus collisions the situation is quite similar. In Fig. 2 we give an example for the chain structure of a nucleus-nucleus collision. There are all together n elementary collisions with n_p projectile and n_t target nucleons involved. For $n_p < n_t$ we have

i. $2n_p$ valence-valence chains $(q_p^v - (qq)_t^v)$ and $((qq)_p^v - q_t^v)$.

ii. $2(n_t - n_p)$ valence-sea chains $(q_p^s - (qq)_t^v)$ and $(\bar{q}_p^s - q_t^s)$.

iii. $2(n - n_t)$ sea-sea chains $(q_p^s - \bar{q}_t^s)$ and $(\bar{q}_p^s - q_t^s)$.

The q^s, $\bar{q}^s$, and q^v and $(qq)^v$ stand here for sea quarks, sea antiquarks, valence quarks and valence diquarks.

The average numbers of collisions n and participating nucleons n_p and n_t depend only weakly the collision energy. However, at low collision energies the invariant masses of many sea-sea chains turn out to be below the masses of the mesons, which could be formed out of the quarks and antiquark at the end of the chains. The kinematics at low collision energies forces the suppression of many sea-sea chains.

If the invariant masses of $q - \bar{q}$ chains are between the masses of the pseudoscalar mesons and vector mesons with the appropriate quark composition we replace the chains by the pseudoscalar mesons and correct the kinematics correspondingly. If the invariant mass of the chains is between the masses of the vector mesons m_v and $m_v + \Delta$ ($\Delta \approx 300$ MeV/c^2), we replace the chains by the vector mesons and correct the kinematics in such a way, that energy and

momentum conservation remain satisfied. In the case of quark-diquark chains we proceed similarly with the octet and decuplet baryons. Chains with masses below the masses of pseudoscalar mesons and octet baryons are suppressed and energy and momentum of the suppressed chains is given to the valence-valence and valence-sea chains.

The distributions of the numbers n, n_A and n_B in collisions of the nuclei A and B follow from Glauber theory. We follow here the formulation and Monte-Carlo algorithms of Zadorozhnyi et al.[14] . The total inelastic collision cross section of the nuclei A and B is given as an integral over the impact parameter b

$$\sigma_{AB}^{inel} = \int d^2b \left\{ 1 - \prod_{i=1}^{A} \prod_{j=1}^{B} [1 - \sigma P_{ij}] \right\} \times \left[\prod_{i=1}^{A} \frac{T_A(\vec{s}_i)}{A} d^2 s_i \right] \times \left[\prod_{j=1}^{B} \frac{T_B(\vec{\tau}_j)}{B} d^2 \tau_j \right] = \int d^2b \, \Gamma(\vec{b}) \tag{1}$$

A and B designate here also the number of nucleons in the nuclei A and B. The vectors $\vec{s}_i$ and $\vec{\tau}_i$ give the positions of the nucleons i and j in the two nuclei. σP_{ij} is given by

$$\sigma P_{ij} = \sigma P(\vec{b} - \vec{s}_i + \vec{\tau}_i) = \gamma(\vec{b} - \vec{s}_i + \vec{\tau}_i) + \gamma^*(\vec{b} - \vec{s}_i + \vec{\tau}_i) - \gamma(\vec{b} - \vec{s}_i + \vec{\tau}_i)\gamma^*(\vec{b} - \vec{s}_i + \vec{\tau}_i) \tag{2}$$

where $\gamma(b)$ is the elastic $N - N$ scattering amplitude as function of the impact parameter b.

The expression for the total inelastic cross section can be written as a sum

over cross sections with ν inelastic nucleon-nucleon interactions

$$\sigma_{AB}^{inel} = \sum_{\nu=1}^{A\cdot B} \sigma_\nu \tag{3}$$

with

$$\sigma_\nu = \frac{(-\sigma)^\nu}{\nu!} \frac{d^\nu}{d\sigma^\nu} \int d^2b \left[\prod_{i=1}^{A} \prod_{j=1}^{B} (1 - \sigma P_{ij}) \right] \times \left[\prod_{i=1}^{A} \frac{T_A(\vec{s}_i)}{A} d^2 s_i \right] \times \left[\prod_{j=1}^{B} \frac{T_B(\vec{\tau}_j)}{B} d^2 \tau_j \right] \tag{4}$$

From this expression Zadorzhnyi et al.[14] work out the algorithm for sampling the events characterized by n, n_A and n_B and by the individual nucleons between which the collisions occur.

In particular for $\nu = 1$ collision one obtains from (4)

$$\sigma_1 = \int d^2b \left[\sum_{i=1}^{A} \sum_{j=1}^{B} \sigma P_{ij} \prod_{\substack{k=1 \\ (k,\ell)\neq(i,j)}}^{A} \prod_{\ell=1}^{B} (1 - \sigma P_{k\ell}) \right] \times \left[\prod_{k=1}^{A} \frac{T_A(\vec{s}_k)}{A} d^2 s_k \right] \times \left[\prod_{\ell=1}^{B} \frac{T_B(\vec{\tau}_\ell)}{B} d^2 \tau_\ell \right] \tag{5}$$

For $\nu = 2$ collisions one obtains terms, where one nucleon of A interacts with two different nucleons of B, where one nucleon of B interacts with two different nucleons of A and finally where two different nucleons of A interact with two different nucleons of B.

$$\sigma_2 = \int d^2b \left\{ \frac{1}{2} \sum_{\substack{i,j=1 \\ i\neq j}}^{A} \sum_{k=1}^{B} \sigma^2 P_{ik} P_{jk} \prod_{\substack{\ell=1 \\ (\ell,m)\neq(i,k),(j,k)}}^{A} \prod_{m=1}^{B} (1 - \sigma P_{\ell m}) \right.$$

$$
\begin{aligned}
&+\frac{1}{2}\sum_{i=1}^{A}\sum_{\substack{j,k=1\\ j\neq k}}^{B}\sigma^2 P_{ij}P_{ik}\prod_{\substack{\ell=1\\ (\ell,m)\neq(i,j),(i,k)}}^{A}\prod_{m=1}^{B}(1-\sigma P_{\ell m})\\
&+\frac{1}{2}\sum_{\substack{i,j=1\\ i\neq j}}^{A}\sum_{\substack{k,\ell=1\\ k\neq \ell}}^{B}\sigma^2 P_{ik}P_{j\ell}\prod_{\substack{m=1\\ (m,n)\neq(i,k),(j,\ell)}}^{A}\prod_{n=1}^{B}(1-\sigma P_{mn})\Bigg\}\\
&\times\left[\prod_{i=1}^{A}\frac{T_A(\vec{s}_i)}{A}\,d^2s_i\right]\times\left[\prod_{j=1}^{B}\frac{T_B(\vec{\tau}_j)}{B}\,d^2\tau_j\right]
\end{aligned}
\tag{6}
$$

The contributions to any number ν of collisions can be constructed and envisaged in a graphical way as indicated in Fig. 3 for $\nu = 1$ and 2.

In Fig. 4, we plot the number of participating projectile nucleons obtained from the Monte-Carlo algorithm for collisions of oxygen and sulfur ions with different nuclei.

Central collisions can be defined as collisions where all nucleons of the projectile nucleus interact. (It is assumed, that the projectile nucleus is lighter than the target nucleus $A_p < A_t$). It is visible from Fig. 4 that a rather large fraction of all collisions is central, provided the target nuclei are heavy enough.

3. THE INTRANUCLEAR CASCADE CORRECTION

At energies well above 3–5 GeV per nucleon the dual multichain fragmentation model provides a picture of multiparticle production in hadron-nucleus and nucleus-nucleus collisions which is superior to the intranuclear cascade mode.[16] In contrast to this, at energies below 3–5 GeV the intranuclear cascade model provides a good description of inelastic nuclear collisions. At these energies the

dual multichain fragmentation model is difficult to apply since most of the quark-antiquark and quark-diquark chains have masses below the masses of the hadrons with the same quark composition. Therefore at these energies this model would mainly be determined by the particular way used to implement the kinematical suppression of the chains.

The physical picture, which explains the absence of the intranuclear cascade at high energies is the concept of the formation zone.[15] Secondary hadrons in the collisions are not formed instantaneously. In their rest frame they need a certain average time τ, which we call the formation time, before they are present as complete hadronic states. Before this time we might understand them in the quark model as states consisting only out of valence quarks, without the full system of sea quarks, antiquarks and gluons. These hadrons have a reduced probability for hadronic interactions inside the nucleus because of the absence of the soft components in the hadronic state.

In this picture it appears to be quite natural, that most of the fast secondaries created in nuclear collisions have no possibility for secondary interactions inside the nucleus. Because of the relativistic time dilatation they are created at positions, where the secondary hadronic system is already outside the nucleus. This explains the absence of the intranuclear cascade at high energies.

The argument for the absence of secondary interactions inside the nucleus applies only to high energy secondary hadrons, not to particles with low energies, which are created inside the target nucleus. This is also consistent with phenomenological observations. For secondary particles with rapidities below $y \approx 2$ in the target rest frame the model predictions were found to be too low com-

pared to the data in our previous[8] study of the dual multichain fragmentation model as applied to hadron nucleus collisions. Starting from these qualitative and phenomenological arguments we propose here a leading order correction to slow secondary particle production in asymmetric collisions ($A_p << A_t$) in the dual multichain fragmentation model. We introduce an empirical parameter τ, which we call the hadronic formation time.

In the dual Monte-Carlo multichain fragmentation model as formulated above we know for each collision event the positions $\vec{s}_i$ and $\vec{r}_j$ of all interacting nucleons in the rest frames of the two nuclei as well as the impact parameter b of the collision. We know also which nucleons are engaged in the elementary collisions. In the model we determine the energies and moments of the secondary particles created. This information gives us the full space-time history of the collisions. In any particular Lorentz frame we can follow the trajectories of the secondaries created in space and time. We choose in particular the target rest frame, which seems to be the natural frame to describe asymmetric collisions of projectile nucleons or light projectile nuclei with heavy target nuclei. In this frame we can trace the trajectory of each secondary hadron with mass m_1 energy E_1 momentum $\vec{p}$ and and Lorentz parameters $\gamma = E/mc^2$ and $\vec{\beta}\gamma = \vec{p}/mc$.

$$\vec{x} = \vec{x}_0 + \dot{\vec{x}}t \qquad ; \qquad \dot{\vec{x}} = \vec{\beta}c \tag{7}$$

We assume that the secondary hadron starts to interact hadronically in its rest frame after the formation time τ or after the time $\tau_t = \gamma\tau$ in the target rest frame. Assuming a target nucleus with fixed radius R we get the time t_{12}, when

the secondary particle leaves the target nucleus from

$$(\vec{x}_0 + \dot{\vec{x}}t)^2 = R^2 \tag{8}$$

or

$$t_R = -\frac{\vec{x}_0 \cdot \dot{\vec{x}}}{\dot{\vec{x}}^2} + \sqrt{\left(\frac{\vec{x}_0 \cdot \dot{\vec{x}}}{\dot{\vec{x}}^2}\right)^2 - \frac{\vec{x}_0^2 - \vec{R}^2}{\dot{\vec{x}}^2}} \tag{9}$$

A particular secondary particle has the chance to interact again inside the nucleus for

$$\tau_i < t_R \tag{10}$$

Since we are only interested in the leading order corrections to the multistring fragmentation model we consider such secondary collisions only for hadrons produced in the primary collision. We do not go on to follow the intranuclear cascade for all low energy hadrons created in turn in the secondary collisions and so on.

It has to be recognized, that the scheme proposed is in no way Lorentz invariant. The conditions for secondary interactions differ if we go into different Lorentz frames, for instance, into the projectile rest frame. In this situation we apply the scheme only to highly asymmetric collisions like hadron-nucleus collisions or nucleus-nucleus collisions with light projectiles as studied, in present experiments.[2,3] We leave for the future the generalization of this scheme to collisions of heavy projectiles and targets and the construction of a full intranuclear cascade for the soft hadrons.

4. THE MONTE-CARLO MODEL

The first step in the generation of each event is the sampling of the positions of all nucleons in the two colliding nuclei, the sampling of the impact parameter and, using the Glauber theory sampling the number of elementary collisions n and participating nucleons n_p and n_t. All this is described in Section 3 and in the paper of Zadorozhnyi et al.[14] .

From the n, n_p and n_t the chain structure of the event is fixed and we sample next the flavors and momentum fractions x of the valence quarks, diquarks and sea quark-antiquark pairs at the end of the chains. It is to be noted, that the x values of the valence and sea quarks to be used in a model for soft particle production are not constrained by the data from deep inelastic lepton-hadron interactions or by other hard hadronic processes. We use for valence quarks the distribution

$$q^{\nu}(x) = \frac{N^{\nu}}{\sqrt{x}}\,(1-x)^2 \tag{11}$$

and for sea quarks and antiquarks

$$q^{s}(x) = \frac{N^{s}}{x}\,(1-x)^6\ . \tag{12}$$

What we really need are the exclusive quark distributions for all valence quarks and diquarks and the k sea quark-antiquark pairs at the end of the chains originating from a given nucleon

$$f(x_q^{\nu}, x_{qq}^{\nu}, x_{q_1}^{s}, x_{\bar{q}_1}^{s}, \ldots x_{q_k}^{s}, x_{\bar{q}_k}^{s}) = q_q^{\nu}(x_q^{\nu}) q_{qq}^{\nu}(x_{qq}^{\nu}) \prod_{i=1}^{k} q^{s}(x_{q_i}^{s}) q^{s}(x_{\bar{q}_i}^{s})$$

$$\times \ \delta\Big(1 - x_q^\nu - x_{qq}^\nu - \sum_{i=1}^{k} (x_{q_i}^s + x_{\bar{q}_i}^s)\Big) \tag{13}$$

We satisfy this distribution by sampling first the x values of all valence and sea quarks from the distributions (11) and (12) and giving at the end to the diquark the x-value

$$x_{qq}^\nu = 1 \ - \ x_q^\nu \ - \ \sum_{i=1}^{k} (x_{q_i}^s + x_{\bar{q}_i}^s) \, . \tag{14}$$

We give also to each multiparticle chain a transverse momentum sampled from the distributions

$$\frac{dn}{p_\perp dp_\perp} \ = \ N \ e^{-BE_\perp} \qquad\qquad E_\perp = \sqrt{p_\perp^2 + m^2} \tag{15}$$

with average transverse momenta in the order of 0.4 GeV/c. The transverse momenta of the two chains which belong to each elementary collision are chosen to be opposite to each other. One of the reasons to give intrinsic transverse momenta to the produced chains is the fact, that very often these chains are found to consist out of one single hadron. Without the chain transverse momenta these single hadrons would be sampled with vanishing transverse momenta.

The next step in the Monte Carlo calculations is the fragmentation of all chains with masses above the masses of the vector mesons and decuplet baryons. These chains are fragmented using the chain decay code BAMJET,[17] which was originally constructed to describe quark-antiquark chains found in hadronic electron-positron events. BAMJET fragments quark-antiquark, quark-diquark and diquark-antidiquark chains into pseudoscalar and vector mesons and octet

and decuplet baryons. Subsequently all hadronic resonances decay, this is sampled using the code DECAY.[18]

Besides the primary elementary collisions of the dual chain fragmentation model we have also to sample the events corresponding to secondary interactions of hadrons with nucleons inside the nucleus as described in Chapter 3. These collisions are at rather low energies, often below 1 GeV. Therefore it is not practical to sample them using again the multichain fragmentation model. We use instead the code HADRIN[19] which samples inelastic hadron-hadron collisions at energies below 5 GeV in good agreement with experiment. HADRIN samples inelastic collisions via quasi two body reactions and subsequent resonance decay.

The complete hadron-nucleus or nucleus-nucleus events are checked by the conservation laws for energy, momentum and additive quantum numbers like charge, strangeness and baryon number. All those conservation laws are satisfied by the individual events sampled.

All distributions presented in this paper are obtained by sampling between 1000 and 2000 events. Depending on the reaction between 2 and 20 min. cpu time on a IBM 3090 computer are needed to create these events.

5. RESULTS AND COMPARISON WITH DATA

The model without the intranuclear cascade correction was already compared to data from oxygen-lead collisions at 200 GeV.[10] Here we want to continue these comparisons and to study the influence of the formation time parameter τ. The τ-parameter will be determined from the comparison to experiments.

The global effect of the formation time correction can be seen from Fig. 5, where we plot the multiplicities of secondary protons, π^+, charged particles and all secondaries in p-Pb and O-Pb collisions as function of τc. The multiplicity of secondary protons (and the multiplicity of neutrons, which behaves quite similar) shows the strongest variation with τ. Most of the additional particles produced by the intranuclear cascade corrections are nucleons. This is consistent with the expectations.

We compare different calculated distributions in nucleon-nucleus collisions with experimental data in order to determine the formation time parameter τ.

i. In Ref. 8 rapidity distributions and rapidity ratios

$$R^A(y) = \frac{dN^{p-A}}{dy} \Big/ \frac{dN^{p-p}}{dy} \tag{16}$$

are calculated in the dual multichain fragmentation model and compared to data in p-Xe collisions at 200 GeV.[20] A disagreement is found at low rapidities in the target rest frame. Above rapidities $y \approx 2$ the agreement of the model and the measured rapidity distributions and rapidity ratios was rather good. At rapidities below $y \approx 2$ the measured rapidity ratios were bigger than the calculated ones.

In Fig. 6 we compare this rapidity ratio calculated with different τc parameters again with the data.[20] The rapidity ratio calculated in[8] corresponds in the present model to the limit $\tau \to 0$, practically, as seen from the multiplicities in Fig. 6 this means $\tau c = 6 - 10$ fm. Now we find a good agreement down to laboratory rapidities of $y = 0$. The optimum formation time parameter in this comparison is

$$\tau c = 1 - 2 \text{ fm} \qquad \text{Rapidity ratios in } p\text{-Xe collisions} \tag{17}$$

ii. The transverse energy distribution $d/dE_\perp$ was measured by the HELIOS (NA 34) Collaboration at the CERN Super Proton Synchrotron[21] in proton-lead collisions. The data are taken in the pseudorapidity range $0.6 \leq \eta \leq 2.4$. In this rapidity range the intranuclear cascade corrections to the model are significant. In Fig. 7 we compare the transverse energy distribution for different τ-values with the data.[21] We find the best agreement for

$$\tau c = 2 - 3 \text{ fm} \qquad (d\sigma/dE_\perp \text{ in } p - \text{Pb collisions}). \tag{18}$$

iii. Transverse energy distributions in p-Au collisions were also measured by the NA 35 Collaboration at the CERN Super Proton Synchrotron.[2] This experiment is sensitive for laboratory rapidities $2.2 \leq y \leq 3.8$. In this rapidity range we do not expect significant changes of the $d\sigma/dE_\perp$ distributions with the τ-parameter. In Fig. 8 we find indeed a good agreement of the model for $\tau c = 1$ fm as well as for $\tau c = 6$ fm with the data. It is not possible to determine the τ-parameter from this experiment. The model agrees well with the data.

We conclude from these three comparisons: The model agrees well with data in nucleon-nucleus collisions. The optimum formation time parameter is around $\tau c = 2$ fm.

Next we compare the model with transverse energy distributions measured in oxygen-nucleus collisions at energies of 200 GeV per nucleon. In Fig. 9 we compare the model with O-Pb data from the NA 35 collaboration at the CERN Super Proton Synchrotron.[2] The data are again for the rapidity range $2.2 \leq y \leq 3.8$. In this rapidity region the model is practically independent on the formation time parameter τ. We find a good agreement of the model with the data.

The transverse energy distribution in oxygen-silver and oxygen-tungsten collisions was measured by the HELIOS collaboration.[3] This experiment is sensitive to pseudorapidities in the range $-0.1 \leq \eta \leq 2.9$. In this range the results of the model depend strongly on the formation time parameter τ. In Fig. 10 we compare the data[3] with the model calculations for $\tau c = 2$ fm and 3 fm. The calculation with $\tau c = 3$ fm agrees better to the data than the one with $\tau c = 2$ fm. This is slightly inconsistent with what we found above from proton-nucleus collisions. We find in both comparisons with oxygen-nucleus collisions presented in Figs. 9 and 10, that the model overestimates somewhat the cross sections at the largest $E_\perp$ values. In order to be more specific what is calculated we specify: For π and K mesons we add for each individual particle $E_\perp = \sqrt{m^2 + p_\perp^2}$ to the $E_\perp$ histograms. For protons and neutrons, which are not identified in the experiments, only the transverse momenta $p_\perp$ are added to the $E_\perp$ histograms. Changes in the model predictions could result from changes in the scattering amplitudes entering in (2) or the nuclear density distributions in (1) and (4). In spite of these small

disagreements we tend to conclude, that the model agrees remarkably well with the experimental data available so far on nucleus-nucleus collisions. From this agreement it can be concluded that these data cannot be interpreted as evidence for new physics like the quark-gluon plasma.

After these comparisons we present some calculated distributions which help to understand the model: In Fig. 11a rapidity distributions are given for hadrons produced in oxygen-lead collisions. The distributions refer to all charged particles, secondary protons and π^--mesons. The secondary proton distribution (and the very similar secondary neutron distribution) shows a remarkable shape. There are two maxima. One maximum at low rapidities corresponds to the fragmentation products of the target nucleus, the second at large rapidity corresponds to the projectile nucleons, which were involved in the inelastic collisions. Such distributions of secondary nucleons have been used to discuss the concept of the nuclear stopping power.[22,23] The dual multistring fragmentation model makes detailed predictions for this.

Central collisions are defined as collisions where all projectile nucleons interact $n_p = A_p$. In Fig. 11b the rapidity distributions resulting from central collisions are presented. Except for the higher overall production no striking qualitative changes are visible as compared to the normal collisions.

In Fig. 12 we compare transverse energy distributions obtained in central collisions with the ones in normal collisions. It can be concluded from this comparison, that the tail of the normal $E_\perp$ distribution results from central collisions. Central collisions offer the best opportunities to find evidence for the formation of the quark-gluon plasma. Events with maximum $E_\perp$ are therefore the most

interesting ones to look for the effects of the quark-gluon plasma.

Finally we present in Fig. 13 transverse momentum distributions obtained in the model for p-Pb and for normal and central O-Pb collisions. All $p_\perp$ distributions look rather similar. It should be stressed, that the model does not incorporate hard hadronic collisions, therefore we expect the model distribution to remain below the data above some sufficiently high transverse momentum. The $p_\perp$ distribution is mainly the result of the $p_\perp$ distribution used in the chain fragmentation model.[17] Slightly below $p_\perp = 1$ GeV/c the slope of the $p_\perp$ distribution of all charged particles changes. This flattening of the $p_\perp$ distribution is due to the secondary protons, which have a larger average $p_\perp$ than pions. This effect is more significant in nucleus-nucleus collisions because of the increased fraction of secondary nucleons in these collisions as compared to hadron-nucleus collisions.

6. ACKNOWLEDGEMENTS

Part of this study was done during a stay at CERN, Geneva, it was completed at the SSC central design group. I would like to thank Dr. K. Goebel at CERN and Prof. M. Tigner at SSC for the hospitality. Acknowledgements are due to Dr. H.-J. Möhring and Dr. S. Ritter, who did collaborate in the first steps of this investigation and due to Dr. S.Yu. Shmakov for discussions and for a FORTRAN program sampling the distribution from Ref. 14.

REFERENCES

1. E. V. Shuryak, Phys. Rep. **61**, 71 (1980); M. Jacob and H. Satz, eds. Quark matter formation and heavy ion collisions. Proc. Bielefeld Workshop, May 1982, Singapore, World Scientific, 1982; R. Hagedorn, Riv. Nuovo Cim. **6**, 1 (1984).
2. A. Bamberger et al., NA35 Collaboration. Phys. Lett. **184**, 271 (1987).
3. Y. Sirois, HELIOS Collaboration, to be published in the Proceedings of the XXII Rencontres de Moriond, March 1987.
4. M. A. Faessler, Ann. Phys. **137**, 44 (1981); S. Fredriksson, G. Eilam, G. Berlad, and L. Bergström, Phys. Rept. **144**, 187 (1987); N. N. Nikolaev, Sov. Phys. Usp. **24**, 531 (1981).
5. J. Ranft and S. Ritter, Z. Phys. **C27**, 413 (1985); J. Ranft, Z. Phys. **C33**, 517 (1987).
6. P. Aurenche, F. W. Bopp and J. Ranft, Z. Phys. **C23**, 67 (1984); P. Aurenche, F. W. Bopp and J. Ranft, Phys. Rev. **D33**, 1867 (1986).

7. J. Ranft and S. Ritter, Z. Phys. **C20**, 347 (1983).

8. J. Ranft and S. Ritter, Z. Phys. **C27**, 569 (1985).

9. H. J. Möhring, J. Ranft and S. Ritter, Z. Phys. **C27**, 419 (1985).

10. J. Ranft, Phys. Lett. **188B**, 379 (1987).

11. A. Capella and J. Tran Thanh Van, Phys. Lett. **93B**, 146 (1980): Nucl. Phys. A **461**, 501c (1987).

12. A. B. Kaidalov and K. A. Ter-Martirosyan, Sov. J. Nucl. Phys. **39**, 979 (1984); A. B. Kaidalov, K. A. Ter-Martirosyan and Yu. M. Shabelskii, Yad. Fiz. **43**, 1282 (1986).

13. A. Capella, C. Pajares and A.V. Ramallo, Nucl. Phys. B, **241**, 75 (1984).

14. A. M. Zadorozhnyi, W. W. Uzhinskii and S. Yu. Shmakov, Dubna preprint P2-86-361 (1986) unpublished.

15. L. Landau and I. Pomeranchuk, Dokl. Akad. Nauk SSR, **92**, 535 (1953); **92**, 734 (1953); E. L. Feinberg, Sov. Phys. JETP **23**, 123 (1966).

16. H. W. Bertini, Phys. Rev. **137**, 1801 (1963); H. W. Bertini, Phys. Rev. **188**, 1711 (1969).

17. S. Ritter and J. Ranft, Acta Phys. Pol. **B11**, 259 (1980); S. Ritter, Z. Phys. **C16**, 27 (1982); S. Ritter, Comput. Phys. Commun. **31**, 393 (1984).

18. K. Hänßgen and S. Ritter, Comput. Phys. Commun. **31**, 411 (1984).

19. K. Hänßgen and J. Ranft, Nucl. Sci. Eng. **88**, 537 (1984).

20. C. De Marzo et al., Phys. Rev. **D26**, 1019 (1982).

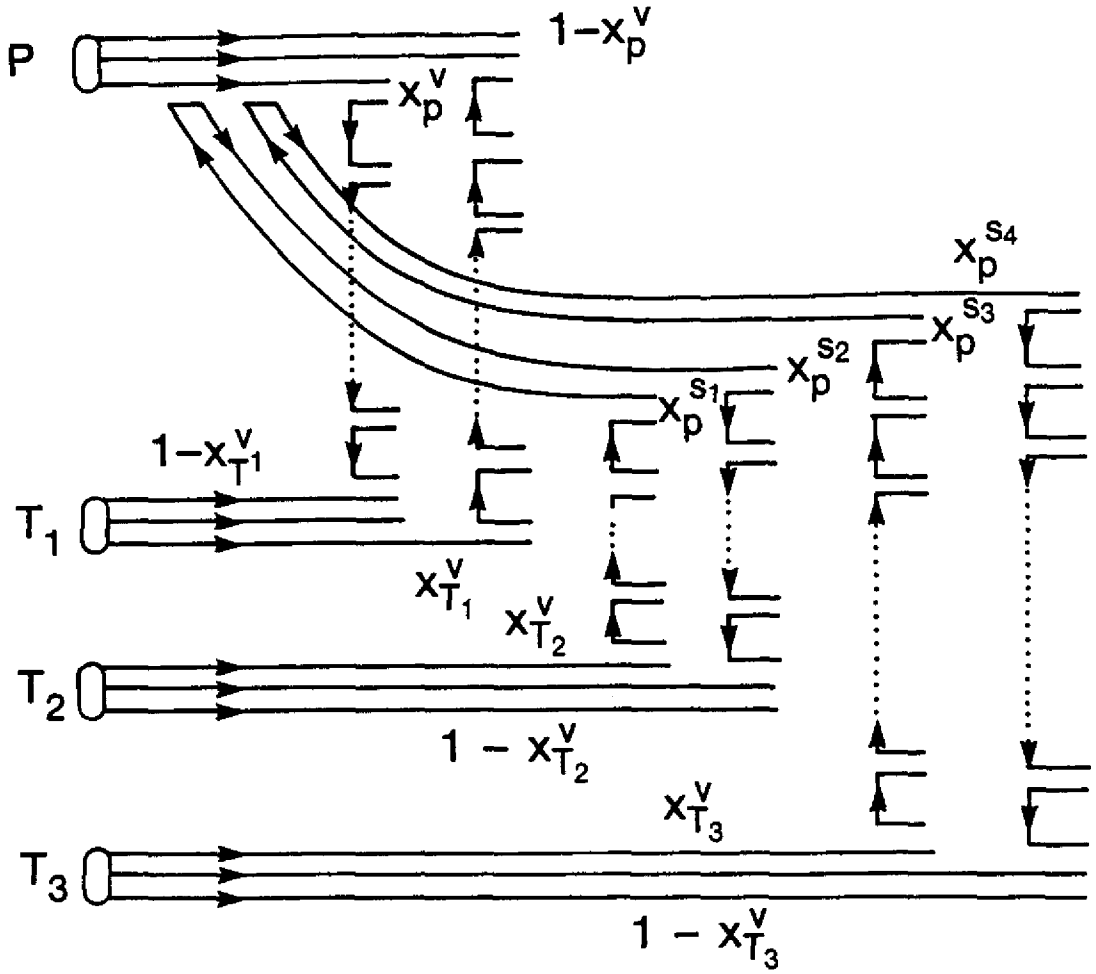

Fig. 1. Example of a triple scattering diagram in a proton-nucleus interaction. P represents the incoming proton and T_1, T_2 and T_3 are three target nucleons taking part in the interaction. x^v and x^{si} are valence and sea-quark momentum fractions.

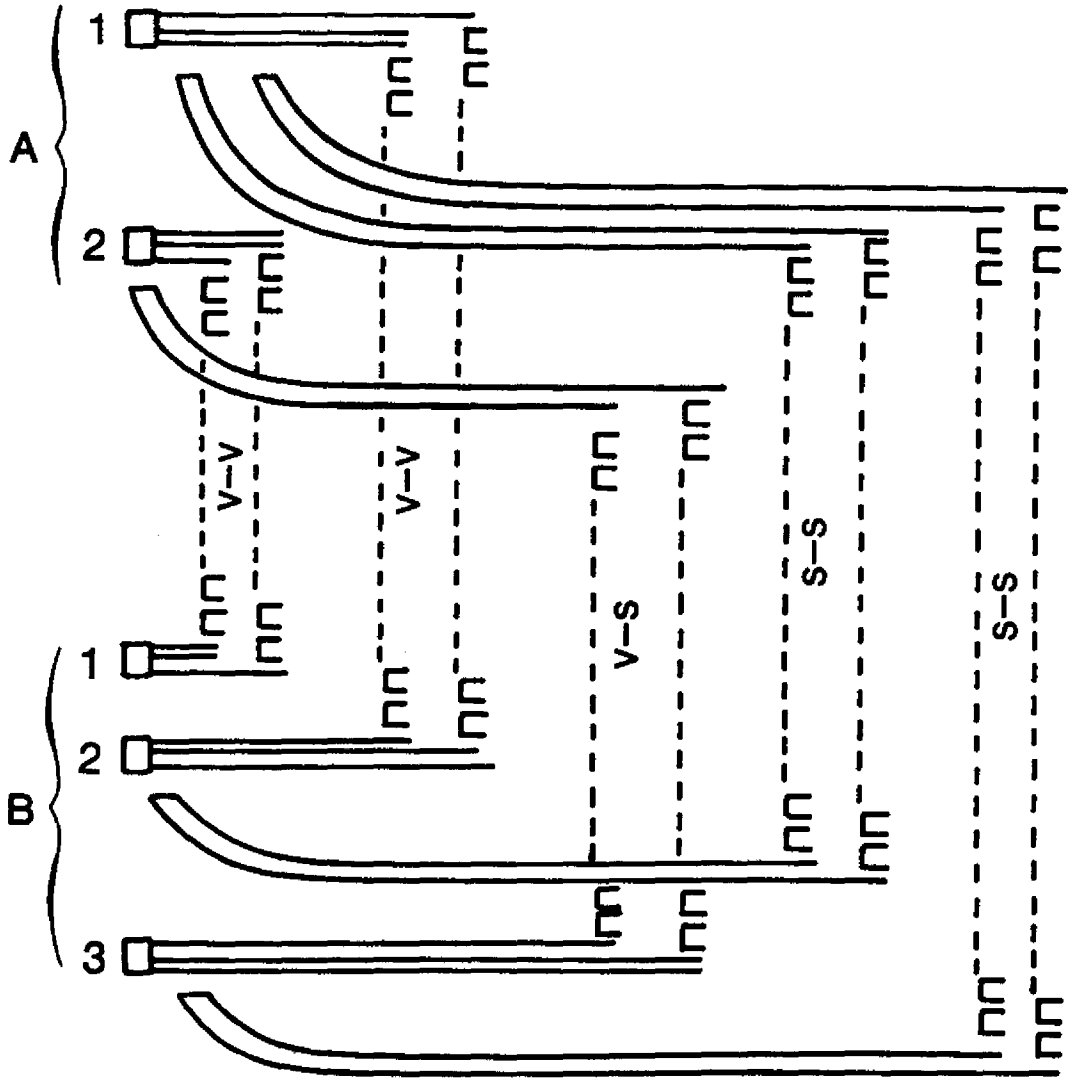

Fig. 2. Example of a nucleus-nucleus scattering process with $n = 5$ interactions and $n_A = 2$ contributing nucleons from the projectile nucleus A and $n_B = 3$ contributing nucleons from the target nucleus B. This gives rise to 4 valence-valence chains, 2 valence-sea chains and 4 sea-sea chains.

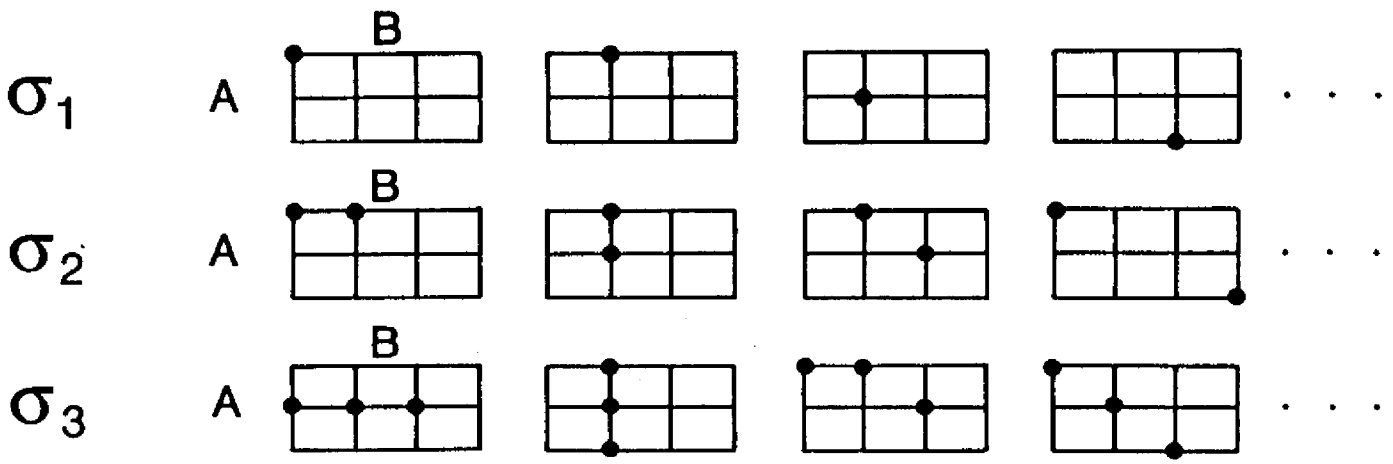

Fig. 3. Graphical representation of some of the contributions to the cross sections with $n = 1, 2$ and 3 elementary scatterings. For $n = 2$ and 3 there are contributions with multiple interactions of one target or projectile nucleon.

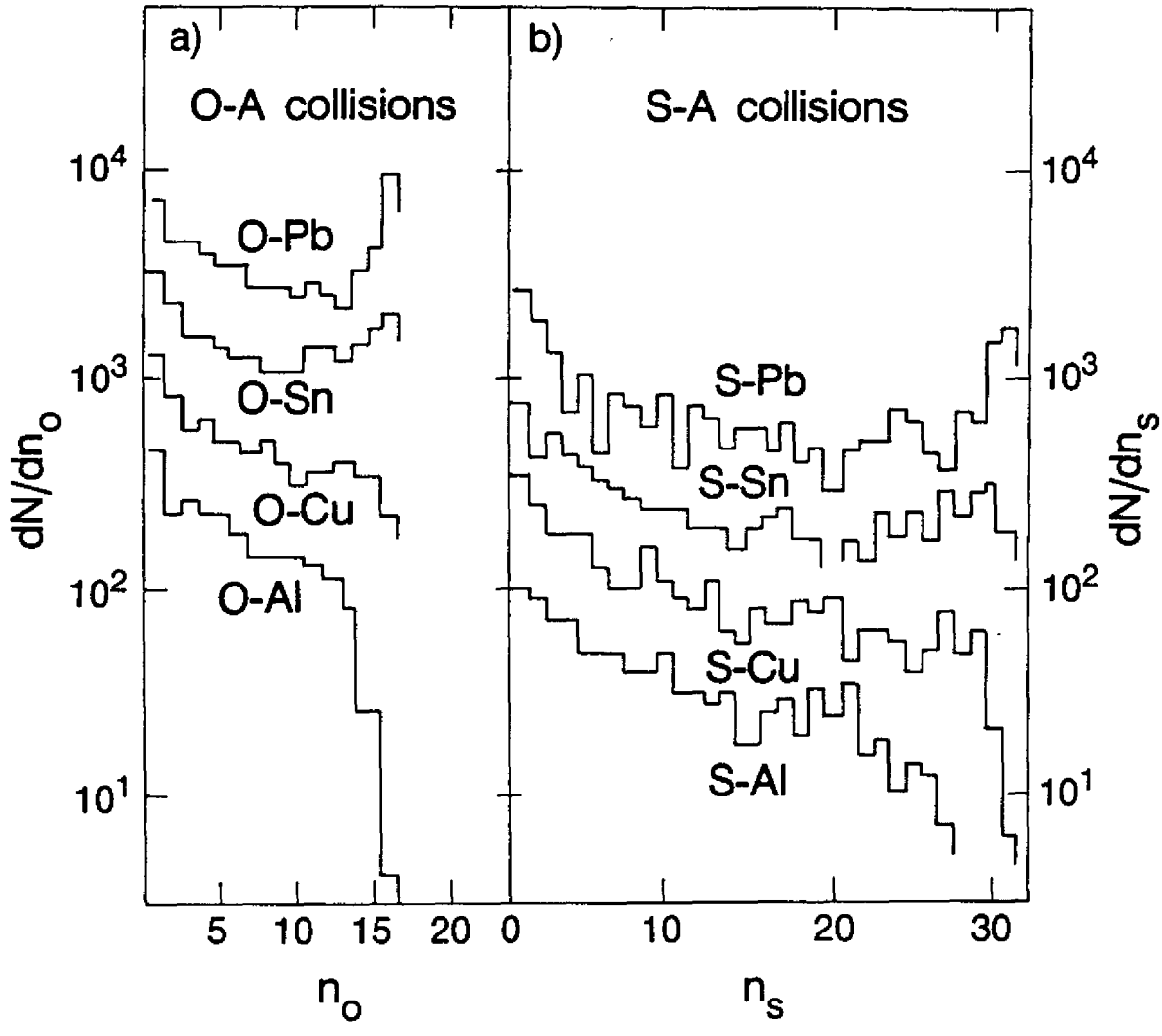

Fig. 4. Distribution in the number of projectile nucleons taking part in collisions of oxygen and sulfur ions with different nuclei. The peaks at $n_O = 16$ and $n_S = 32$ correspond to central collisions. a) O-A collisions, b) S-A collisions.

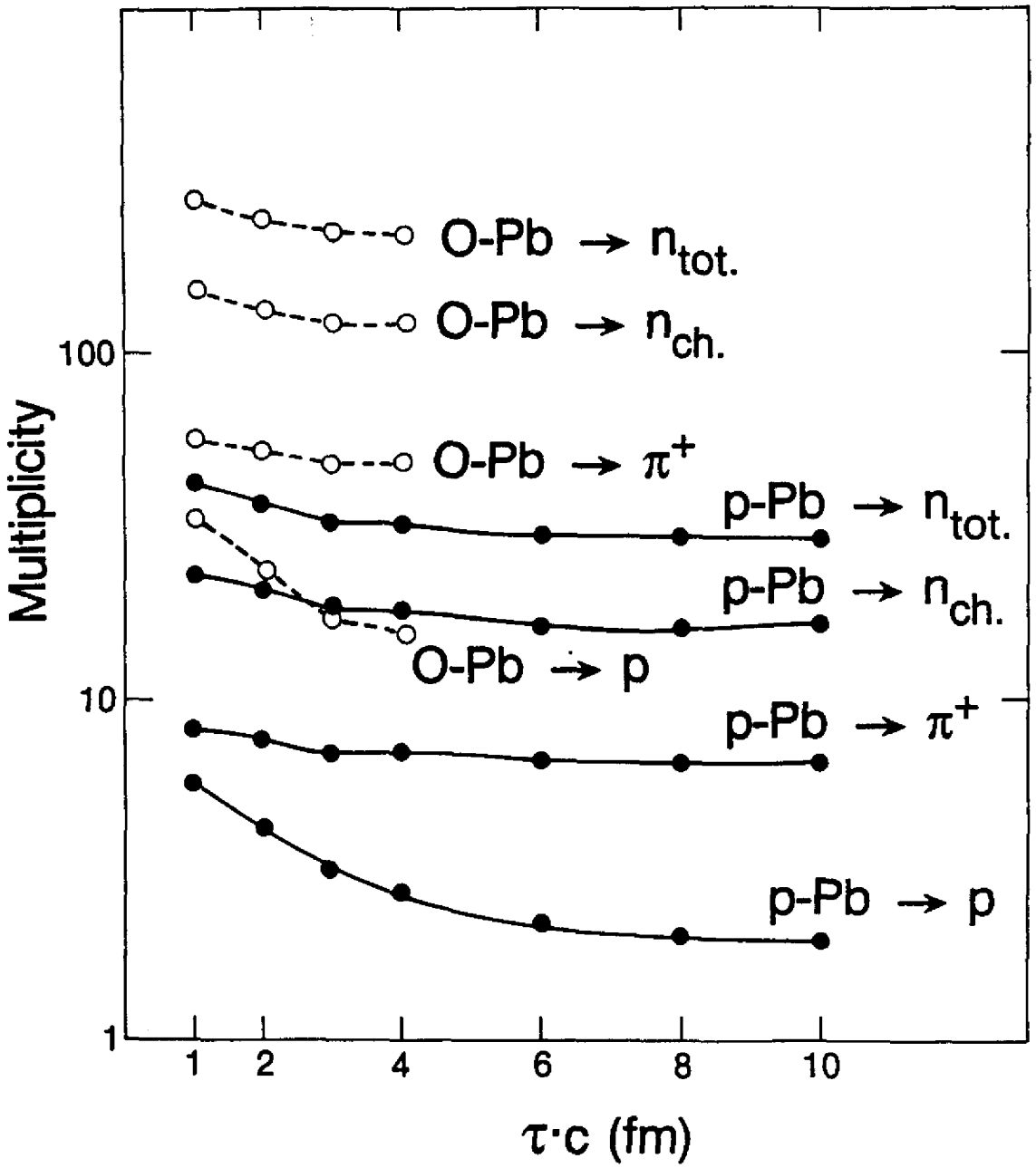

Fig. 5. Multiplicities of secondary protons, π^+, charged hadrons and all produced particles in p-Pb and O-Pb collisions as function of the formation time parameter $\tau \cdot c$.

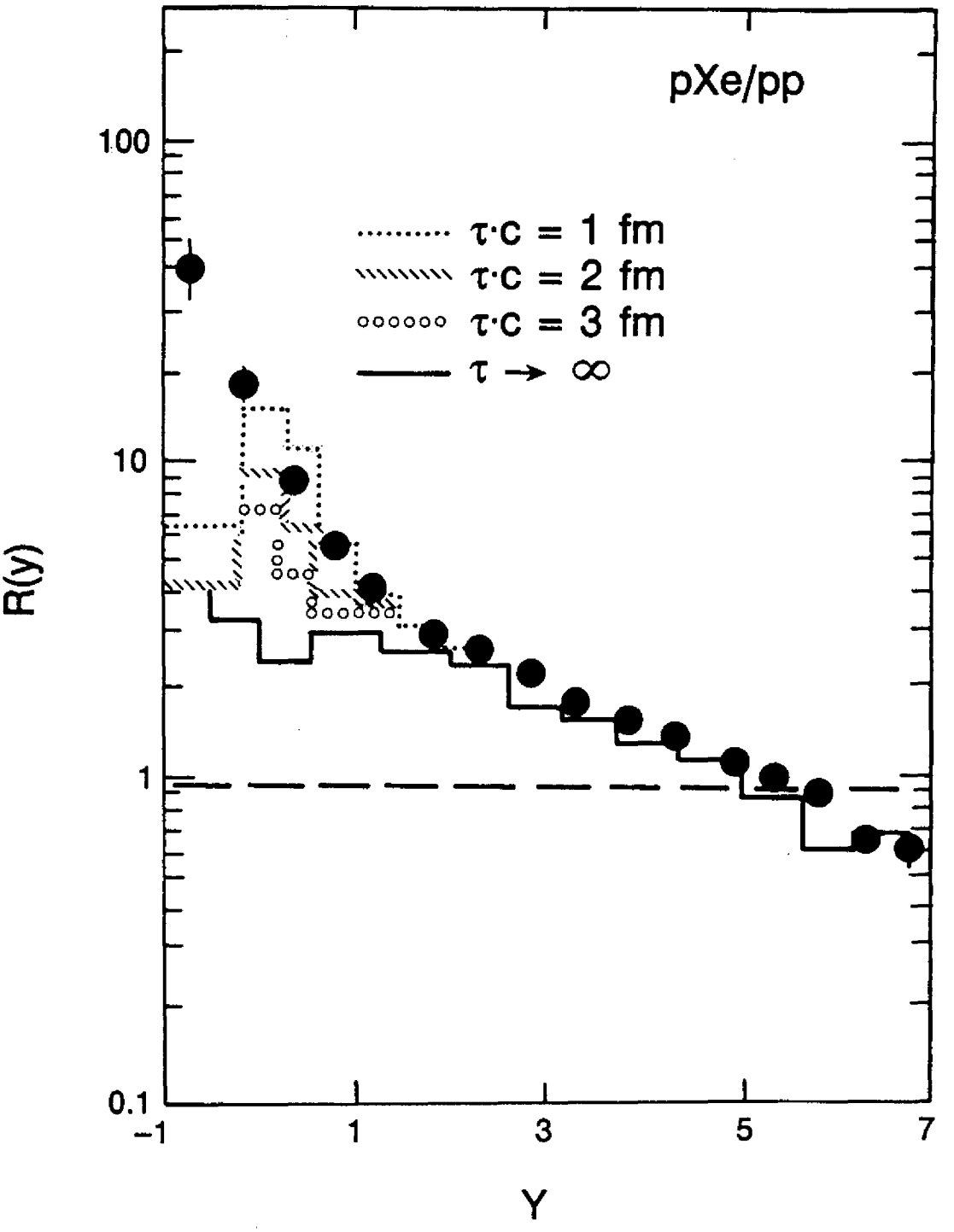

Fig. 6. Rapidity ratios $R(y) = [dN/dy(p - \mathrm{Xe})]/[dN/dy(p - p)]$ for all charged particles at proton energies in the laboratory frame $p_{Lab} = 200$ GeV/c. The Monte-Carlo results represented by histograms are compared to data from [20]. The lowest histogram corresponding to $\tau \to \infty$ was already calculated in [8].

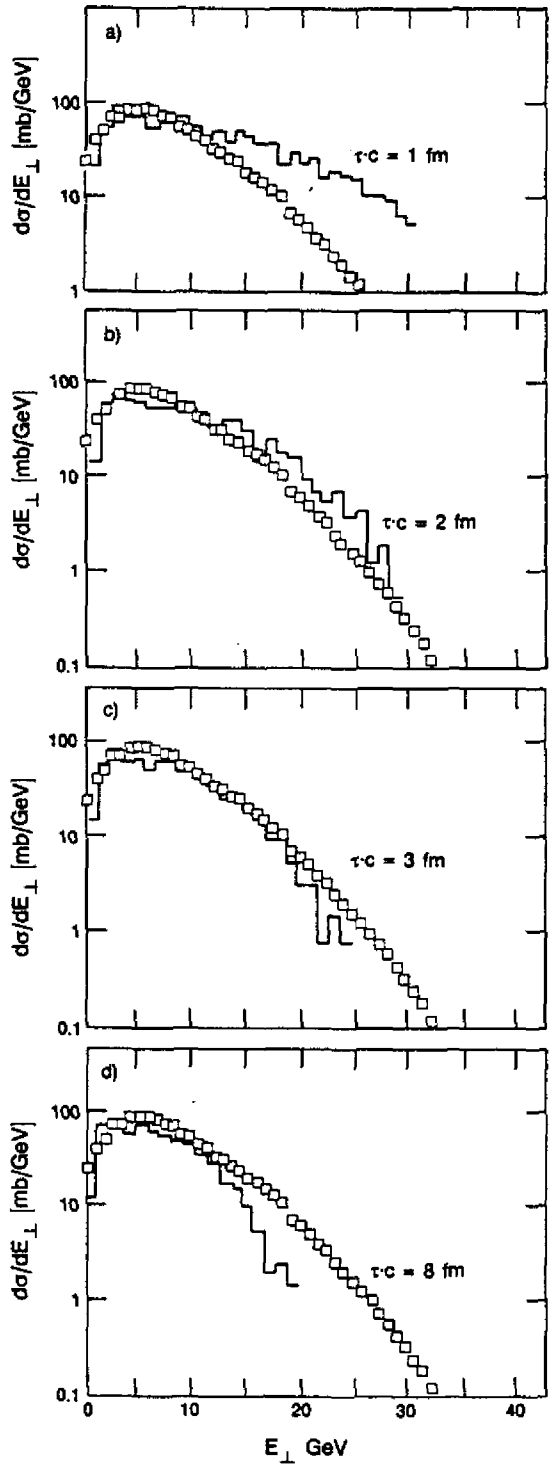

Fig. 7. Transverse energy distributions $d\sigma/dE_\perp$ for protons interacting on Pb nuclei. The calculations given by histograms are compared to data (points) from the HELIOS Collaboration [21] measured in the pseudorapidity range $0.6 \leq \eta \leq 2.4$. The calculation was done with different formation time parameter $\tau \cdot c$. (a) $\tau \cdot c = 1$ fm, (b) $\tau \cdot c = 2$ fm, (c) $\tau \cdot c = 3$ fm, (d) $\tau \cdot c = 8$ fm.

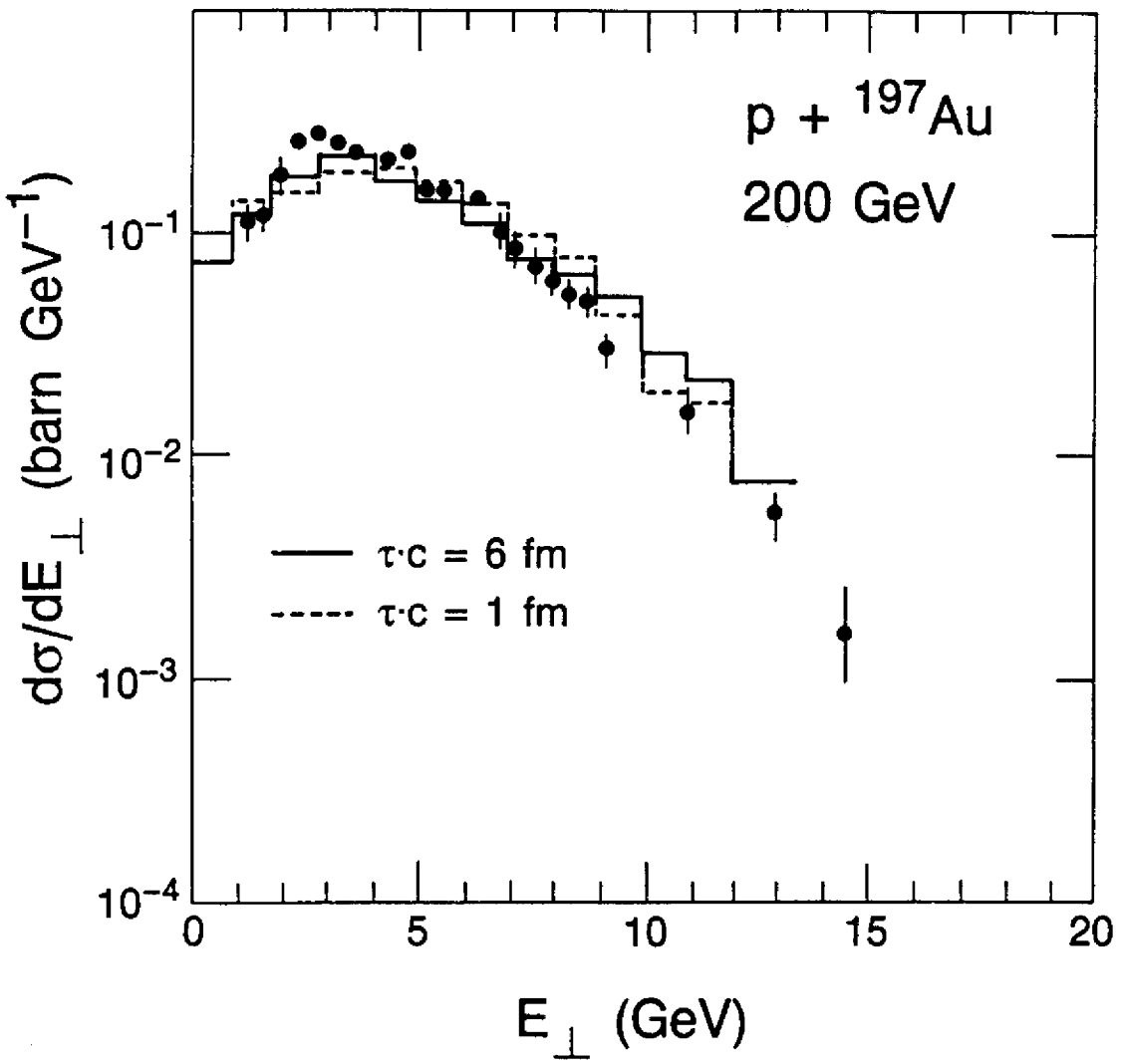

Fig. 8. Transverse energy distributions $d\sigma/dE_\perp$ for protons interacting on Au nuclei. The calculations given by histograms are compared to data (points) from the NA35 Collaboration [2] measured in the rapidity range $2.2 \leq \eta \leq 3.8$. The Monte Carlo results are presented for two different values of the formation time parameter τ.

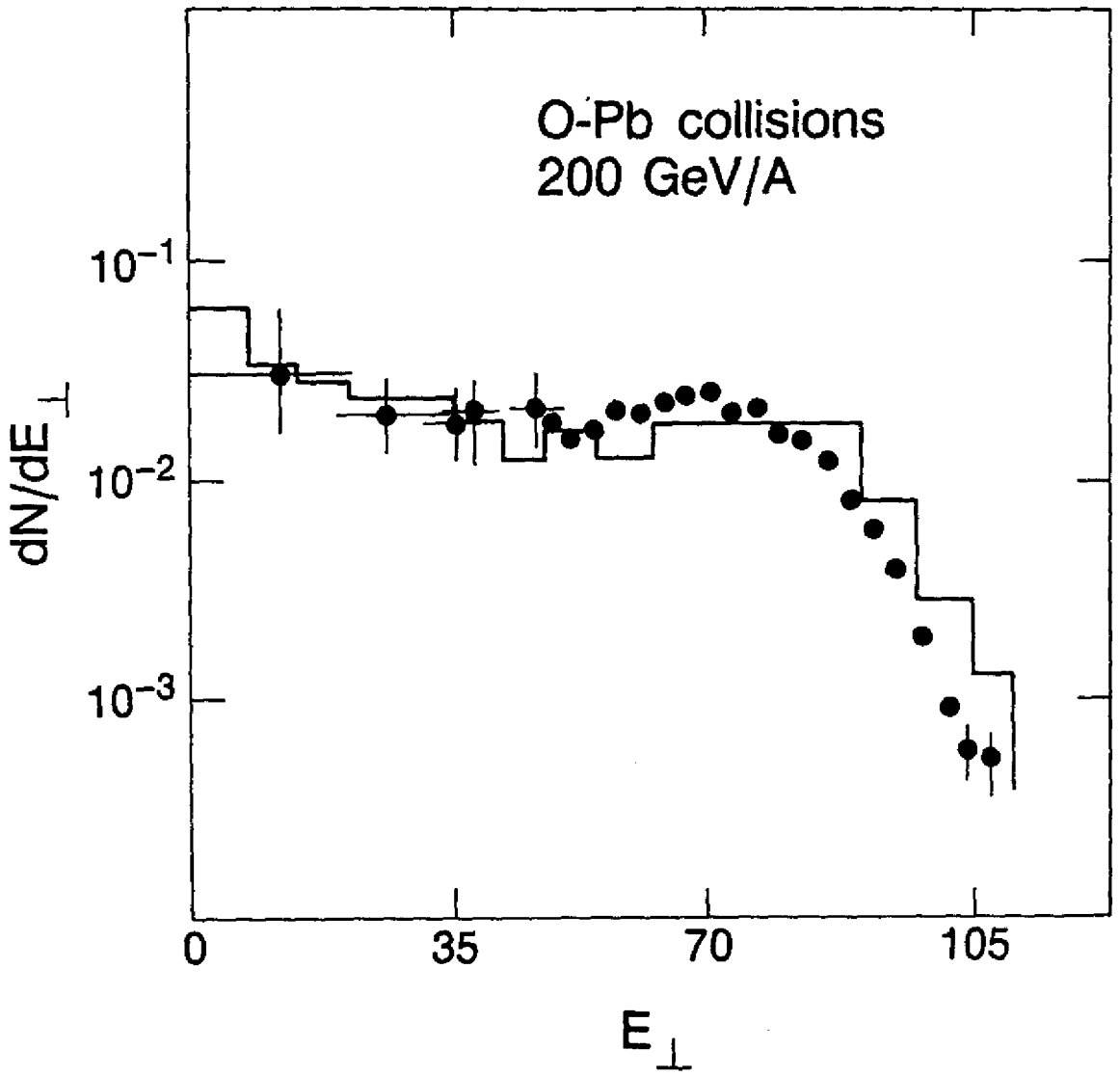

Fig. 9. The transverse energy distribution in O-Pb collisions with 200 GeV per nucleon. The results of the model (histogram) are compared with experimental data (points) from the NA35 Collaboration [2].

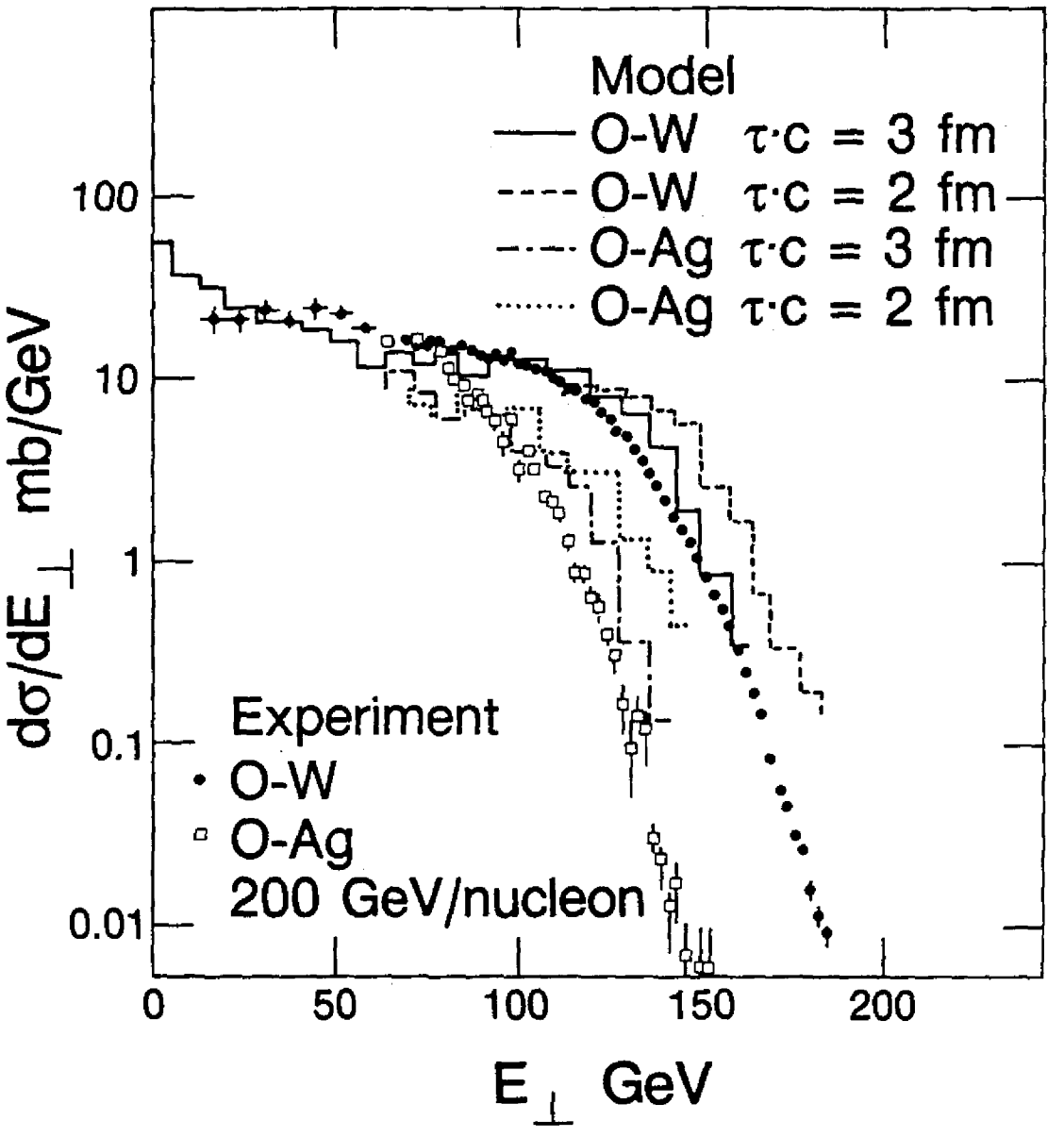

Fig. 10. Transverse energy distributions in O-Ag and O-W collisions with 200 Gev per nucleon. The results of the Monte-Carlo calculation (histograms) are compared with experimental data (points) of the HELIOS-collaboration [3]. The model results are given for two values of the formation time parameter τ.

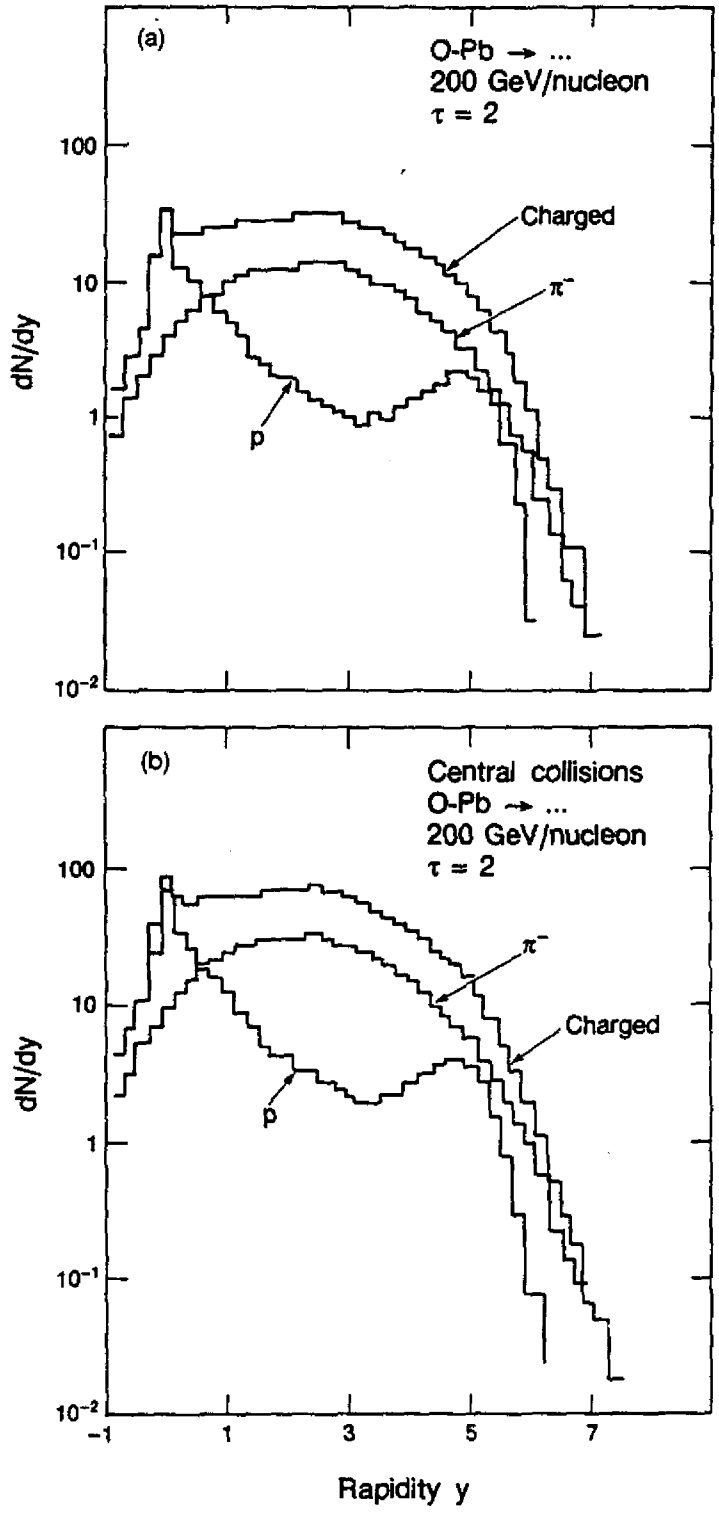

Fig. 11. Rapidity distributions of secondary protons, π^--mesons and all charged particles in O-Pb collisions with 200 GeV per nucleon as calculated by the model. (a) normal collisions, (b) central collisions only.

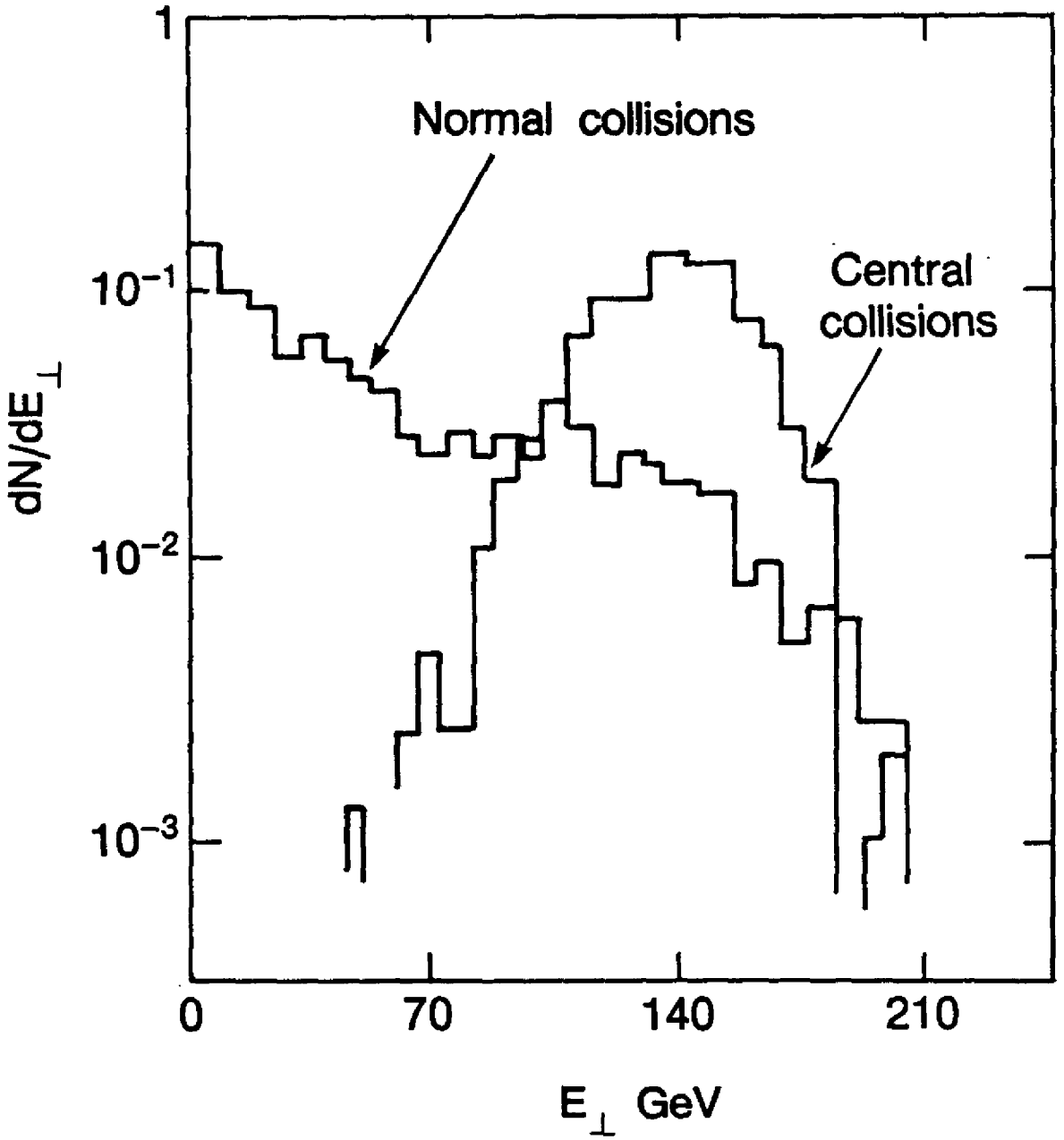

Fig. 12. Transverse energy distributions as calculated for normal and central collisions with a formation time parameter $\tau \cdot c = 2$ fm for all secondaries in the rapidity range $-0.1 \leq \eta \leq 2.9$ for O-Pb collisions.

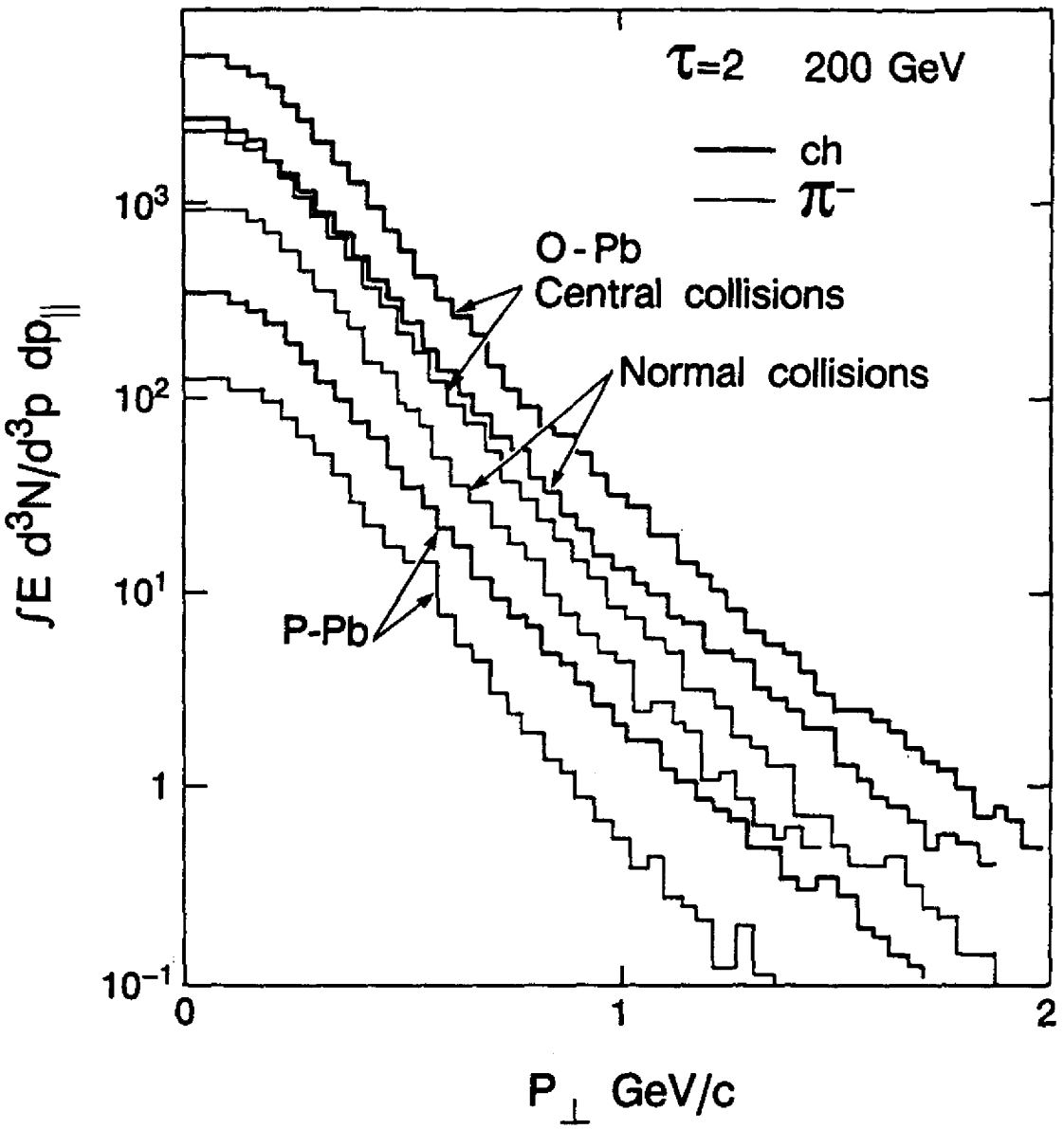

Fig. 13. Transerve momentum distributions of all charged particles and π^- mesons as calculated for p-Pb and normal and central O-Pb collisions.